Damping of pressure waves in visco-elastic, saturated bubbly magma

I. KURZON[1,2], V. LYAKHOVSKY[2], O. NAVON[1] & N. G. LENSKY[2]

[1]*Institute of Earth Science, The Hebrew University, Jerusalem 91904, Israel (e-mail: ittai.kruzon@mail.huji.ac.il)*

[2]*The Geological Survey of Israel, 30 Malkhe Israel St., Jerusalem 95501, Israel*

Abstract: The attenuation of pressure waves in a saturated bubbly magma is examined in a model, coupling seismic wave-propagation with bubble growth dynamics. This model is solved analytically and numerically, including effects of diffusion of volatiles, visco-elasticity and bubble number density. We show that wave attenuation is controlled mainly by the *Peclet* and *Deborah* numbers. The *Peclet* number is a measure of the relative importance of advection to diffusion. The *Deborah* number is a visco-elastic measure, describing the importance of elasticity in comparison to viscous melt deformation. We solve numerically for wave attenuation for various magma properties corresponding to a wide range of *Peclet* and *Deborah* numbers. We show that the numerical solution can be approximated quite well for frequencies above 1 Hz, by an analytical end-member solution, obtained for high *Peclet* and low *Deborah* numbers. For lower frequencies, volatile transport should be accounted for, leading to higher attenuation with respect to the analytical solution. However, if the *Deborah* number is increased, either by longer relaxation time or by higher frequencies, then attenuation decreases with respect to the analytical solution. Therefore, visco-elasticity leads to a significant improvement of the resonating qualities of a magma-filled conduit and widens the depth and frequency ranges where pressure waves will propagate efficiently through the conduit.

The interaction of pressure waves with bubbly liquids has been discussed in the literature. It was confronted either by studying non-linear radial oscillations of a single bubble (Keller & Kolodner 1956; Keller & Miksis 1980; accounting also for liquid compressibility — Prosperetti & Lezzi 1986; Lezzi & Prosperetti 1987; and including the effect of heat transfer between bubble and liquid — Prosperetti *et al.* 1988) or by exploring linear pressure waves in bubbly liquids (Caflisch *et al.* 1985*a*,*b* present a rigorous mathematical approach while Commander & Prosperetti 1989 present a more heuristic approach following the suspension-model of Van Wijngaarden 1968). Commander & Prosperetti (1989) focused on linear pressure waves propagating in liquids containing small concentrations of gas bubbles. They constrained their treatment to conditions of no volatiles flux between bubble and melt, and to wavelengths that are much longer than the typical radius of bubbles.

Ichihara *et al.* (2004) presented a model accounting for effects of bubble resonance and scattering of pressure waves propagating through a visco-elastic bubbly liquid. This model was further developed by Ichihara & Kameda (2004) to include also thermal effects and non-ideality of the gas in the bubble on the acoustic bulk properties of a bubbly magma.

The problem of mass transfer between bubbles and melt in volcanic systems was confronted by Collier *et al.* (2006) in order to obtain the attenuation of pressure waves propagating through a magma-filled conduit, assuming an incompressible bubbly magma. They concluded that there is a very limited range in depth which allows waves to propagate with minimum damping.

In this study, we integrate the theory of pressure waves propagating in bubbly liquids (Commander & Prosperetti 1989) with the theory of bubble growth in magmas (Navon & Lyakhovsky 1998). Analytical solutions are presented (Table 1) for four bubble-growth end-member regimes: viscous, diffusive, equilibrium and no mass flux. Visco-elasticity and melt compressibility are introduced by a new visco-elastic bubble growth model. This model is used to generate a visco-elastic, numerical solution for the Q factor, and to understand better the physics of seismic-wave attenuation in a saturated, visco-elastic bubbly magma.

Theory

The wave equation for bubbly liquids

Commander & Prosperetti (1989) studied the propagation of pressure waves through a mixture

From: LANE, S. J. & GILBERT, J. S. (eds) *Fluid Motions in Volcanic Conduits: A Source of Seismic and Acoustic Signals*. Geological Society, London, Special Publications, **307**, 11–31.
DOI: 10.1144/SP307.2 0305-8719/08/$15.00

Table 1. *The general structure of this paper*

Analytical solutions for the viscous model				Numerical solutions
No mass flux (NMF) regime	Viscous regime	Diffusive regime	Equilibrium regime	
Low-viscosity Compressible (equation 25)				
Incompressible (equation 26)		Incompressible (equation 36)	$Q \to \infty$ (equation 38)	Incompressible, Viscous (Fig. 4)
Compressible (equation 24)	Compressible (equation 30)	Compressible (equation 35)	$Q \to \infty$ (equation 38)	Visco-elastic (Fig. 5)

Generalization to the finite shell model (equations 39–42)
The relations between the numerical and analytical solutions (Figs 4, 5)
The dependency of damping on the *Peclet* number (Figs 5, 7)
The dependency of damping on n_d, f_E and *De* (Fig. 6)
Analytical approximations for the visco-elastic numerical solution (Fig. 8)
The visco-elastic $Q(f, depth)$ profile of a magma-filled conduit (Fig. 9)

of liquid and gas bubbles. They simplified the expressions for the continuity and momentum equations of a mixture and derived from them the following wave equation (see Appendix A for a detailed description):

$$\frac{1}{c^2}\ddot{\delta P} - \nabla^2 \delta P = \rho_m \ddot{\phi}, \tag{1}$$

where $\delta P(x, t)$ is the amplitude of the pressure wave (which is small in comparison to the ambient pressure); ρ_m and c are the density and speed of sound in the melt. The variable ϕ stands for the gas volume fraction and is defined as

$$\phi = \frac{4}{3}\pi R^3 n_d, \tag{2}$$

where R is the bubble radius and n_d is the number density (number of bubbles in a unit volume of the bubbly magma) which is assumed constant for $\phi \ll 1$.

We search for a solution to (1) assuming the following expression for a propagating wave:

$$\delta P(x, t) = A \exp(ikx - i\omega t), \tag{3}$$

Table 2. *Constants and parameters used in the model*

Constants/parameters	Symbol	Value
P-wave velocity in melt	c	2300 m/s
Melt density	ρ_m	2300 kg/m^3
Bulk modulus	K	12 GPa
Solubility constant	K_H	4.11×10^{-6} Pa$^{-1/2}$
Molecular weight of water	M	0.018 kg/mol
Ideal gas constant	G	8.314 J/(mol · K)
Melt temperature	T	1123 K
Wave amplitude	δP	0.1 MPa
Applied frequency	f	**0.0001–1000 Hz**
Number density	n_d	**10^{12} m^{-3}–10^{15} m^{-3}**
Initial pressure	P_0	**20 MPa–80 MPa**
Initial radius	R_0	**0.1 μm–10 μm**
Diffusivity	D	**10^{-12} m^2/s–10^{-10} m^2/s**
Viscosity	η	**10^5 Pa · s–10^8 Pa · s**
Shear modulus	μ	**0.1 GPa–1 GPa**

The values are based mainly on Collier *et al.* (2006) and Hurwitz & Navon (1994). The viscosity range accounts for the effective viscosity, considering the possibility of a high-viscosity skin around growing bubbles (Lensky *et al.* 2001; Mourtada-Bonnefoi & Mader 2001). The shear modulus range is based on Mungall *et al.* (1996), Romano *et al.* (1996) and Dingwell (1998).

where ω is the angular frequency of the propagating pressure wave, k is the related wave number and A is the slowly changing wave-amplitude. Understanding the attenuation of such waves is the main aim of this paper.

The Q *factor*

Commonly, attenuation is expressed by the quality factor, Q, describing how well a system could maintain its oscillatory motion. Of several expressions suggested in the literature, the most frequently used has been defined by Aki & Richards (2002):

$$Q = \frac{2\pi E(\omega)_{\max}}{\Delta E(\omega)}, \tag{4}$$

where ω is the angular frequency of the wave, $E_{\max}$ is the maximum energy stored in one cycle at a specific frequency and ΔE is the energy dissipated in one cycle. O'Connell & Budiansky (1978) obtained Q through the constitutive equation of a visco-elastic medium:

$$Q = \frac{\left|\mathrm{Re}M(\omega)\right|}{\left|\mathrm{Im}M(\omega)\right|}, \tag{5}$$

where $M(\omega)$ is the complex elastic modulus of the material. In this definition, Q refers to the ratio between the real and imaginary parts of the complex modulus.

Collier *et al.* (2006) modified the definition given by (5) and obtained the following definition for Q:

$$Q(\omega) = \frac{\left|\mathrm{Re}V_{bm}^2\right|}{\left|\mathrm{Im}V_{bm}^2\right|} = \frac{1}{\tan(\psi)}. \tag{6}$$

This expression indicates that the *Q factor* could be obtained by two methods: either by the ratio between the real and imaginary parts of V_{bm}, the complex wave velocity in the bubbly magma, or by ψ, the phase lag between the applied stress and the resulting strain rate.

Saturated bubbly magma

We assume that for a saturated bubbly magma, bubble radius oscillates around its initial saturation value, R_0, and that the amplitude of the oscillations is small ($\delta R(x, t) \ll R_0$). For constant R_0 we may write that:

$$\begin{aligned} R &= R_0 + \delta R(x,t) \\ \dot{R} &= \dot{\delta R}(x,t) \\ \ddot{R} &= \ddot{\delta R}(x,t). \end{aligned} \tag{7a–c}$$

Furthermore, solving for small oscillations we assume that

$$R^3 \cong R_0^3 + 3R_0^2\delta R. \tag{8}$$

We substitute (8) into (2), differentiate ϕ twice with respect to time (assuming constant n_d and ρ_m) and substitute the resulting expression into (1) leading to

$$\frac{1}{c^2}\ddot{\delta P} - \nabla^2\delta P = \rho_m 4\pi n_d R_0^2\,\ddot{\delta R}. \tag{9}$$

Equation 9 is the fundamental wave equation of our model, describing pressure waves in a saturated bubbly magma. This equation should be combined with the pressure-dependent δR, derived from the bubble growth model, in order to obtain a full solution for wave propagation and attenuation.

Bubble growth dynamics

The growth of bubbles in a liquid is controlled by two main processes. The first process is the diffusion of dissolved volatiles from a supersaturated melt into bubbles after decompression or from bubbles into an undersaturated melt under compression. The second process is the visco-elastic deformation of the melt. Proussevitch *et al.* (1993) suggested that the bubbly magma can be modelled as a grid of closely packed spherical cells, where each cell includes a spherical bubble enclosed by a finite shell of melt. Assuming that there is no interaction between the cells, modelling of one cell provides a general solution for the bubble growth process. The cell model was further developed by Proussevitch & Sahagian (1996), Lyakhovsky *et al.* (1996), Navon & Lyakhovsky (1998) and Lensky *et al.* (2004), showing good agreement with experimental results.

Since bubble growth dynamics is essential for the present study, we present below a brief description of the model. The model assumes a Newtonian incompressible fluid, with spherical symmetry and using spherical coordinates.

Consider a bubble of radius R_0 in equilibrium with a melt shell of radius S_0 at pressure P_0. Water mass balance dictates that

$$R_0^3 = S_i^3(C_i - C_0)\frac{\rho_m}{\rho_g}. \tag{10}$$

where ρ_g is the gas density, C_i is the water concentration in the melt when the bubble dissolves and shrinks, leaving a melt sphere of radius S_i ($S_i^3 = S^3 - R^3$) and C_0 is the equilibrium water

concentration. C_0 (and any other equilibrium concentration) is related to the pressure through the solubility law of water, that for pressures up to 200 MPa, is commonly approximated as a square-root relation:

$$C_0 \approx K_{\mathrm{H}}\sqrt{P_0}, \tag{11}$$

where K_{H} is Henry's constant.

If pressure is changed to a new pressure $P_a \neq P_0$, the system is no longer in equilibrium and volatiles diffuse through the melt and transfer to or from the bubble according to:

$$\frac{d\left(\frac{4}{3}\pi R^3 \rho_g\right)}{dt} = 4\pi D \rho_m R^2 \left(\frac{\partial C}{\partial r}\right)_R, \tag{12}$$

where D is the diffusivity of water in the melt and C is the water concentration in the melt.

The concentration gradient at the interface is obtained by solving the diffusion-advection equation:

$$\frac{\partial C}{\partial t} + v(r)\frac{\partial C}{\partial r} = \frac{1}{r^2}\frac{\partial}{\partial r}\left(Dr^2\frac{\partial C}{\partial r}\right), \tag{13}$$

where $v(r)$ is the radial melt velocity. For an infinite shell and quasi-static concentration profile, the concentration gradient on the bubble-melt interface is (Lyakhovsky *et al*. 1996):

$$\left(\frac{\partial C}{\partial r}\right)_R = \frac{(C_0 - C_R)}{R}, \tag{14}$$

where C_R is the concentration of volatiles on the bubble-melt interface, and C_0 is the equilibrium pressure on the outer boundary of the shell.

The gas density in the bubble is related to pressure by the ideal gas law:

$$\rho_g = \frac{M}{GT}P_g, \tag{15}$$

where M is the molecular weight of water, G is the gas constant and T is the absolute temperature, which is assumed constant in this model. For an infinite shell, P_a, P_g and $v(r)$ are related by the momentum and continuity equations:

$$\frac{\dot{R}}{R} = \frac{1}{4\eta}(P_g(t) - P_a(t)), \tag{16}$$

where η is the viscosity of the melt and

$$v(r) = \dot{R}\frac{r^2}{R^2} \tag{17}$$

Navon & Lyakhovsky (1998) showed that following an instantaneous pressure drop, three regimes can be identified (Fig. 1): (i) a viscous regime where diffusion is efficient, gas pressure is maintained close to P_0 and bubble growth is controlled mainly by viscous deformation; (ii) a diffusive regime where gas pressure falls so that P_g is close to P_a, and growth is controlled mainly by diffusion; and (iii) an equilibrium regime where melt and bubbles approach chemical equilibrium and R approaches equilibrium at $P = P_a$.

The different growth regimes can be characterized with the following timescales (Fig. 1): $\tau_V = 4\eta/(P_0 - P_a)$ for the viscous growth; $\tau_D = R_0^2/D$ for the diffusive growth and $\tau_E = S_i^2/D$ for reaching equilibrium. In cases where diffusive mass transfer is negligible, an additional timescale is defined: $\tau_{NMF} = 4\eta/3P_0$ (Barclay *et al.* 1995), where NMF stands for 'No Mass Flux'. These timescales, and especially the relations between them, provide the key for understanding the dependency of damping on the various processes occurring in the bubbly magma. Furthermore, the inverse of these time scales can be related to the frequency of pressure waves propagating through a bubbly magma.

The model discussed above accounts for viscous deformation of the melt neglecting the elastic component of melt deformation; this assumption is allowed for low Deborah numbers: $De \equiv \eta\dot{\tau}/\mu\tau < 1$, where μ is the shear modulus of the melt, τ is the applied stress and $\dot{\tau}$ is the rate of stress-loading. This number corresponds to the ratio between the Maxwell relaxation time $\tau_m = \eta/\mu$ and the characteristic time of loading $\tau/\dot{\tau}$, and reflects the nature of deformation in the material. For propagating waves (according to (3) $\tau/\dot{\tau} = 1/\omega$ and the Deborah number is expressed as $De = \omega\eta/\mu$. For a magma with constant η and μ, De is proportional to the frequency of the applied pressure wave. For low frequencies, $De < 1$, deformation is viscous and elastic strains are negligible. At very high frequencies, $De \gg 1$, deformation is mostly elastic and viscous components could be ignored. For $De \approx 1$, elastic and viscous components should be considered, and for an infinite shell we obtain two additional terms in the momentum equation:

$$\frac{\dot{R}}{R} = \frac{1}{4\eta}\left(P_g(t) - P_a(t)\right) + \frac{1}{4\mu}\frac{d\left(P_g(t) - P_a(t)\right)}{dt} - \frac{1}{3K}\frac{dP_a(t)}{dt}. \tag{18}$$

(See Appendix B for the full derivation.) The first term in the right-hand side of the equation stands for viscous resistance (as in equation 16), the

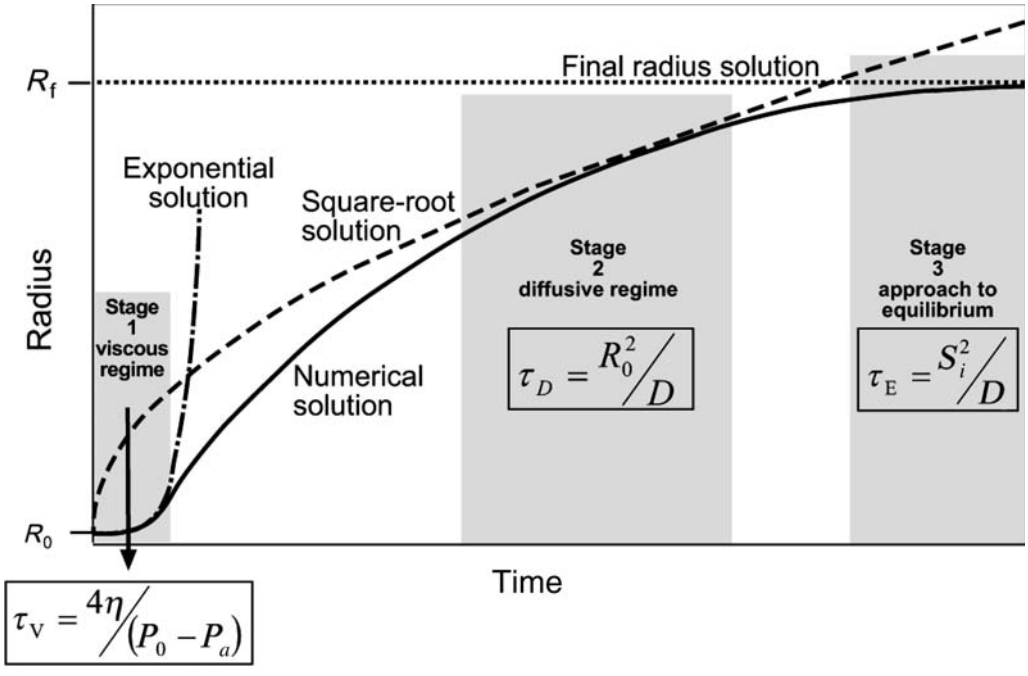

Fig. 1. Bubble growth solutions as a function of time (after Lensky *et al.* 2002). The numerical solution corresponds to the analytical end-member growth regimes. Also seen are the characteristic timescales for growth (see text for further explanation).

second term is the elastic component and the third term accounts for melt compressibility.

Analytical solutions

The Q *Factor for No Mass Flux (NMF) conditions: a benchmarking study*

The 'No Mass Flux' approximation describes bubble growth dynamics when diffusion of volatiles between melt and bubbles is negligible; this is actually the case solved by Commander & Prosperetti (1989). Since we are considering small vesicularities, we will focus our treatment on the infinite shell model, when the bubble does not 'see' the outer boundary of the shell. A generalization to a finite shell is given in Appendix C.

The no mass flux condition states that the mass of gas in the bubble is constant:

$$P_g R^3 = P_0 R_0^3. \tag{19}$$

Substitution of (8) in (19) yields

$$P_g \approx \frac{P_0 R_0^3}{R_0^3 + 3R_0^2 \delta R} \approx P_0\left(1 - 3\frac{\delta R}{R_0}\right). \tag{20}$$

Substitution of (20), (7a) and (8) in (16) leads to the following expression:

$$\frac{\dot{\delta R}(t)}{R_0} = \frac{1}{4\eta}\left[P_0\left(1 - 3\frac{\delta R(t)}{R_0}\right) - P_a(t)\right]. \tag{21}$$

Defining $P_a(t) = P_0 + \delta P(t)$, the solution for this equation becomes:

$$\delta R(t) = \exp\left[-\frac{t}{\tau_{NMF}}\right] \times \left\{\int -\frac{R_0}{4\eta}\exp\left[\frac{t}{\tau_{NMF}}\right]\delta P(t)dt\right\}. \tag{22}$$

Taking the second derivative of (22) in respect to time, substituting the result into (9) and applying (3) leads to the following equation for the inverse of the complex phase velocity:

$$\frac{1}{V_{bm}^2} = \frac{1}{c^2} + \frac{\rho_m \pi n_d R_0^3 (1 + i\omega\tau_{NMF})\tau_{NMF}}{\eta (1 + \omega^2 \tau_{NMF}^2)}. \tag{23}$$

Following the Quality factor definition (6), we obtain the following expression for $Q(\omega)$:

$$Q = \frac{\eta\omega}{\rho_m \pi n_d R_0^3 c^2} + \frac{1}{\omega} \cdot \left[\frac{9P_0^2}{\rho_m 16\eta\pi n_d R_0^3 c^2} + \frac{3P_0}{4\eta} \right]. \tag{24}$$

Commander & Prosperetti (1989) obtained a similar solution. However, since in their treatment they accounted only for fluids of low viscosity (e.g. water), the first term was naturally neglected, resulting in:

$$Q = \frac{1}{\omega} \cdot \left[\frac{9P_0^2}{\rho_m 16\eta\pi n_d R_0^3 c^2} + \frac{3P_0}{4\eta} \right]. \tag{25}$$

This equation is similar to the one obtained by Collier *et al.* (2006). For an incompressible fluid, with $c \to \infty$, this expression could be simplified even more giving:

$$Q = \frac{3P_0}{4\eta\omega}. \tag{26}$$

The solutions for the compressible case (24) and the incompressible case (26), along with the low viscosity solution of Commander & Prosperetti (25) are presented in Figure 2a.

Magma rheology: Kelvin versus Maxwell visco-elasticity. The analytical NMF solutions allow a first peek into magma rheology. By examining the general equation (24), we may note that for low frequencies $Q \propto 1/\omega$ — the quality factor decreases with increasing frequency, and damping increases. This effect could be explained by Kelvin's model for a visco-elastic material (a spring and dashpot in parallel, see Fig. 3). In this model, the elastic response of the material is retarded and viscous response is more dominant in the initial moments of applied stresses. Therefore, when frequency increases the elastic component becomes less dominant, allowing viscous dissipation to control the oscillations and to enhance damping. At higher frequencies, damping decreases with increasing frequency and $Q \propto \omega$. This part of the solution indicates a behaviour according to Maxwell's model for a visco-elastic material (a spring and a dashpot in series, see Fig. 3). In this model, a visco-elastic material will initially react elastically before continuing its response by viscous flow. As the period of the applied stress is reduced (frequency increases), elastic response dominates the behaviour of the material and damping is reduced.

The full solution (24) is typical for a standard linear solid (Malvern 1969; Aki & Richards 2002) and may be presented by the three-element model (two springs and a dashpot, see Fig. 3). This solution reflects the double role of the shear viscosity in relation to the elastic properties of a fluid. High viscosity means high resistance to flow, and thus high loss of energy when the material is flowing. On the other hand, when a material becomes very viscous it approaches an elastic behaviour, allowing elastic waves to propagate without loss of energy.

At low frequencies, viscous flow is the main actor in melt deformation (Kelvin's model); therefore $Q(\omega) \propto 1/\eta$ and the role of viscosity is pronounced in the dissipation of elastic energy. At high frequencies, viscous flow hardly contributes to melt deformation and viscosity leads to domination of the elastic nature of the material (Maxwell's model) and reduction of energy loss. With this basic physical insight into magma rheology, we may proceed and add diffusion to our system. We first present analytical end-member solutions and then the results of the numerical simulations.

The Q *Factor for mass flux conditions*

Collier *et al.* (2006) obtained a numerical solution for Q in an incompressible, viscous, bubbly magma with diffusive mass flux between melt and bubbles. They adjusted the bubble growth numerical code of Lyakhovsky *et al.* (1996) to obtain the phase lag, ψ (6), and resulting Q factor. When mass flux between bubbles and melt is allowed, the three regimes controlling the change in bubble volume (viscous, diffusive and equilibrium) provide the following end-member analytical solutions:

Viscous regime. Viscous resistance controls growth when diffusion is efficient and succeeds in keeping the initial gas pressure in the bubble close to P_0. Under such conditions, the momentum equation (16) is the governing equation, and since $P_a(t) = P_0 + \delta P(t)$ it becomes

$$\frac{\dot{R}}{R} = -\frac{1}{4\eta}\delta P(t). \tag{27}$$

We differentiate (27) in respect to time and use (7) to obtain an expression for $\ddot{\delta R}$. We substitute this expression into (9) and obtain:

$$\frac{1}{c^2}\ddot{\delta P}(t) - \nabla^2 \delta P(t) = -\frac{\rho_m \pi n_d R_0^3}{\eta}\dot{\delta P}(t). \tag{28}$$

Applying (3) we obtain an expression for the complex phase velocity as:

$$\frac{1}{V_{bm}^2} = \frac{1}{c^2} + i\frac{\rho_m \pi n_d R_0^3}{\eta\omega} \tag{29}$$

and the related $Q(\omega)$ factor becomes

$$Q(\omega) = \frac{\omega\eta}{\rho_m \pi n_d R_0^3 c^2}. \tag{30}$$

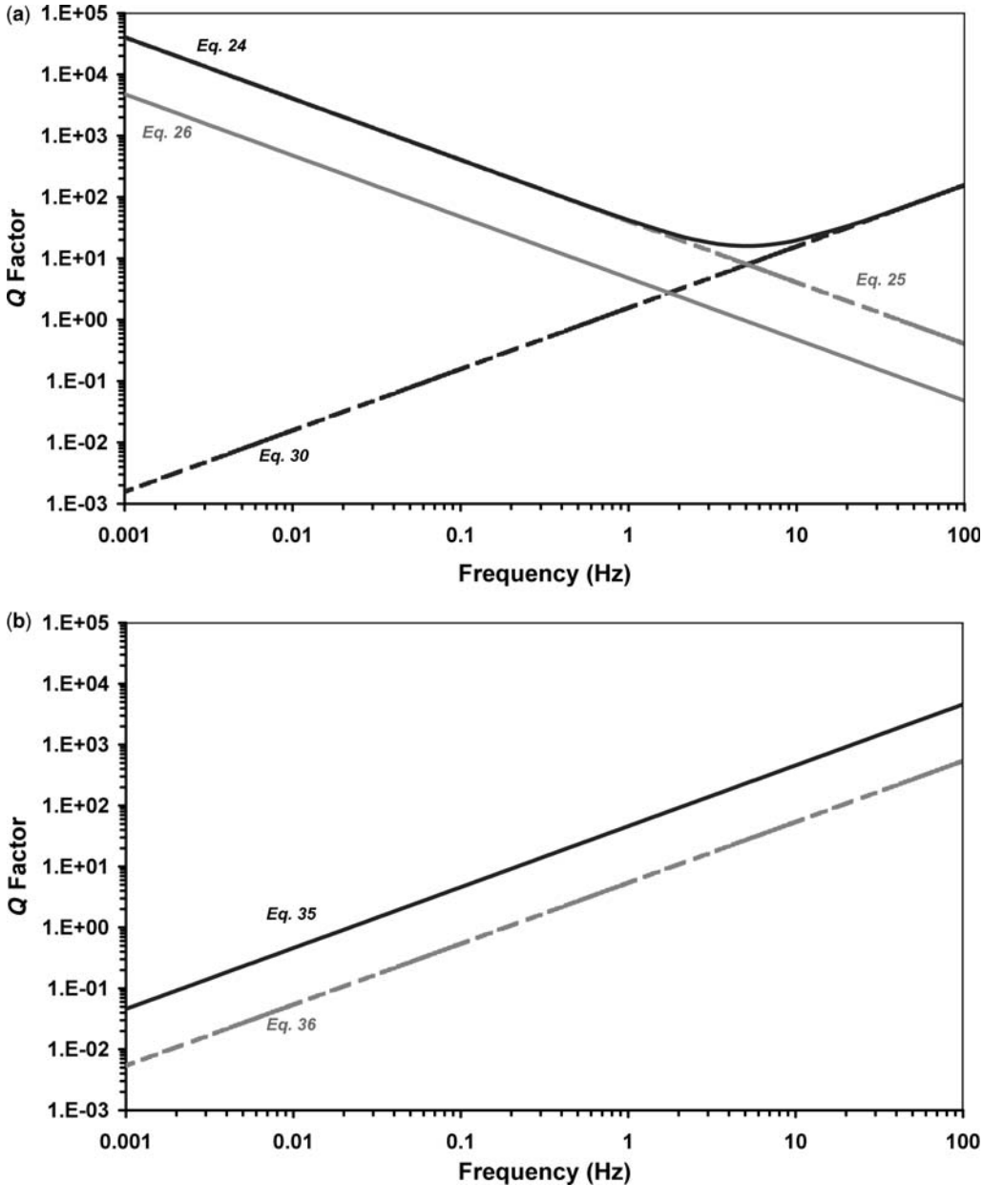

Fig. 2. Analytical solutions. (**a**) The NMF and viscous analytical solutions of $Q(f)$. The dashed black line stands for the viscous solution (equation 30); the grey dashed line for the low viscosity NMF solution (equation 25); the grey continuous line for the incompressible NMF solution (equation 26) and the black continuous line for the compressible NMF solution (equation 24). (**b**) The diffusive analytical solutions for $Q(f)$. The dashed grey line represents the solution for an incompressible melt (equation 36) and the continuous black line for a compressible melt (equation 35). *Magma properties*: $P_0 = 40$ MPa; $R_0 = 1$ μm; $D = 10^{-12}$ m^2 s^{-1}; $\eta = 10^6$ Pa · s; $n_d = 10^{14}$ m^{-3}.

This expression for Q is identical to the first term of (24) and is presented in Figure 2a. Here $Q \propto \eta$, as the role of viscosity is preventing bubble growth (or shrinkage), so it plays only one of its roles: pronouncing the elastic behaviour of the material (Maxwell).

Diffusive regime. The diffusive regime is reached when diffusion cannot compensate for growth and the gas pressure in the bubble approaches the ambient pressure. Using (12), for the water mass balance and (14), for the concentration gradient in

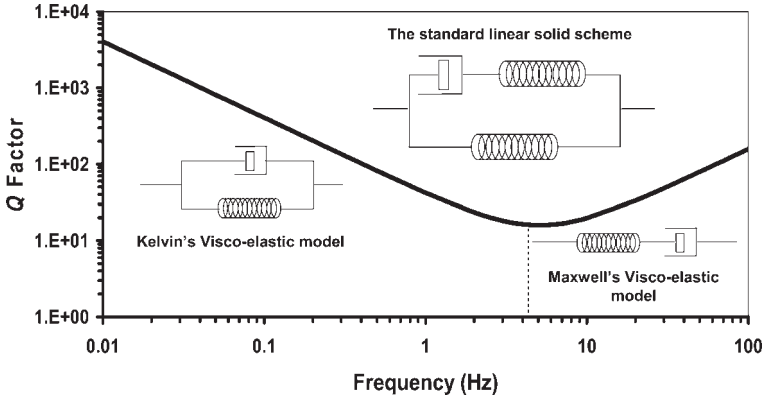

Fig. 3. Magma rheology: Kelvin versus Maxwell visco-elasticity. The visco-elastic model reflected by the compressible NMF solution and described by the spring and dashpot schemes. The two opposite trends ($Q \propto 1/\omega$ and $Q \propto \omega$) are related, respectively, to Kelvin's and Maxwell's visco-elastic model. The two trends add up to give the standard linear solid scheme. Magma properties are as in Figure 2.

the shell, we get the following expression:

$$\frac{d}{dt}\left(\left(R_0^3 + 3R_0^2\delta R\right)\rho_g\right) = 3D\rho_m(R_0 + \delta R)(C_0 - C_R). \tag{31}$$

For $C_0 - C_R$ we apply the solubility equation (11) approximating for $\delta P \ll P_0$, and obtain

$$C_0 - C_R \approx -C_0\frac{\delta P}{2P_0}. \tag{32}$$

Solving for small oscillations controlled by diffusive regime, we may approximate $P_g \approx P_a \approx P_0$, and $\rho_g \approx \rho_0$. Substitution of (15) and (32) in (31) leads to

$$\dot{\delta R} = -\frac{D\rho_m C_0}{R_0\rho_0}\frac{\delta P}{2P_0} - \frac{R_0}{3P_0}\dot{\delta P}. \tag{33}$$

Differentiation of (33) and substitution into (9) yields the following wave equation:

$$\frac{1}{c^2}\ddot{\delta P} - \nabla^2\delta P = \rho_m 4\pi n_d R_0^2\left[-\frac{D\rho_m C_0}{R_0\rho_0}\frac{\dot{\delta P}(t)}{2P_0} - R_0\frac{\ddot{\delta P}(t)}{3P_0}\right] \tag{34}$$

leading to

$$Q(\omega) = \omega\frac{2R_0^2\rho_0}{3\rho_m DC_0} + \omega\frac{P_0\rho_0}{2\pi c^2\rho_m^2 DR_0 n_d C_0} = \omega\frac{2R_0^2\rho_0}{3\rho_m DC_0}\left(1 + \frac{P_0}{c^2\rho_m\phi}\right). \tag{35}$$

This solution reflects the major aspect regarding the addition of diffusion into the system. The process of diffusion increases the loss of energy in the system due to the additional energy consumed by the deformation of the viscous melt around the oscillating bubbles (Collier *et al.* 2006). Therefore, $Q(\omega) \propto 1/D$ and as frequency increases diffusion is less dominant leading to a decrease in damping and higher Q. Additional aspects of diffusion will be discussed below.

For an incompressible melt, the second term of (35) vanishes, and

$$Q(\omega) = \omega\frac{2R_0^2\rho_0}{3\rho_m DC_0}. \tag{36}$$

These $Q(\omega)$ solutions (equations 35, 36) are presented in Figure 2b.

Equilibrium regime. The equilibrium growth regime occurs whenever bubbles and melt manage to maintain chemical equilibrium, even if the ambient pressure varies. In the context of this study, equilibrium is approached for very low-frequency pressure waves propagating through a bubbly magma. At equilibrium, bubble radius is defined by the mass balance equation (10), using an expression analog to (32) for $C_i - C_f$:

$$3R_0^2\delta R(t) = -\frac{S_i^3 C_i\rho_m}{2\rho_0 P_0}\delta P(t). \tag{37}$$

Double differentiation of (37) and substitution into (9) yields the following wave equation:

$$\left[\frac{1}{c^2} + \frac{2\pi\rho_m^2 S_i^3 n_d C_i}{3\rho_0 P_0}\right]\ddot{\delta P} + k^2\delta P = 0. \tag{38}$$

Equation 38 describes a harmonic oscillator without any damping term; this is expected, when assuming the system is in chemical equilibrium. Therefore, the phase lag between applied stress and resulting strain approaches zero and $Q \to \infty$.

Numerical solutions

The numerical simulation of attenuation covers the whole range of Q between the analytical end-member solutions presented above. In order to improve our perception of the numerical solutions, we will proceed in two steps. First, we present a simulation of an incompressible, viscous melt and compare it with the analytical solutions in order to explain the numerical results of Collier *et al.* (2006). Secondly, we present the more general visco-elastic solution (where we account for melt compressibility) and explain it using the analytical solutions and the incompressible, viscous numerical solution.

An incompressible, viscous melt

We applied the numerical code (Lyakhovsky *et al.* 1996; Collier *et al.* 2006) and obtained the Q factor using the phase lag, ψ, between applied stress and resulting strain (6). This version of the code is applicable only for an incompressible viscous melt, hence the results where compared with the analytical solutions for an incompressible melt (Fig. 4). As expected from the analytical solutions, at very low frequencies, when bubbles and melt manage to maintain chemical equilibrium, Q approaches infinity (to the left of the frequency range presented in Figure 4). As frequency increases and the efficiency of diffusion in attaining chemical equilibrium is reduced, more energy is consumed for each cycle and damping increases. This trend reaches a local minimum at frequencies close to $f_E = 1/\tau_E = D/S_i^2$, the equilibrium growth frequency-scale. Beyond this frequency, diffusion does not manage to maintain equilibrium over S_i, (S_i represents the approximate length-scale that diffusion must affect in order to approach chemical equilibrium). This behaviour reflects an additional role of diffusion in maintaining chemical equilibrium. Higher D leads to higher f_E and to higher Q values at frequencies below f_E.

Above f_E, the diffusion process becomes only an additional consumer of energy, and like in the diffusive analytical solution, as frequency increases so damping decreases. This trend continues up to the frequency where Q approaches the NMF analytical

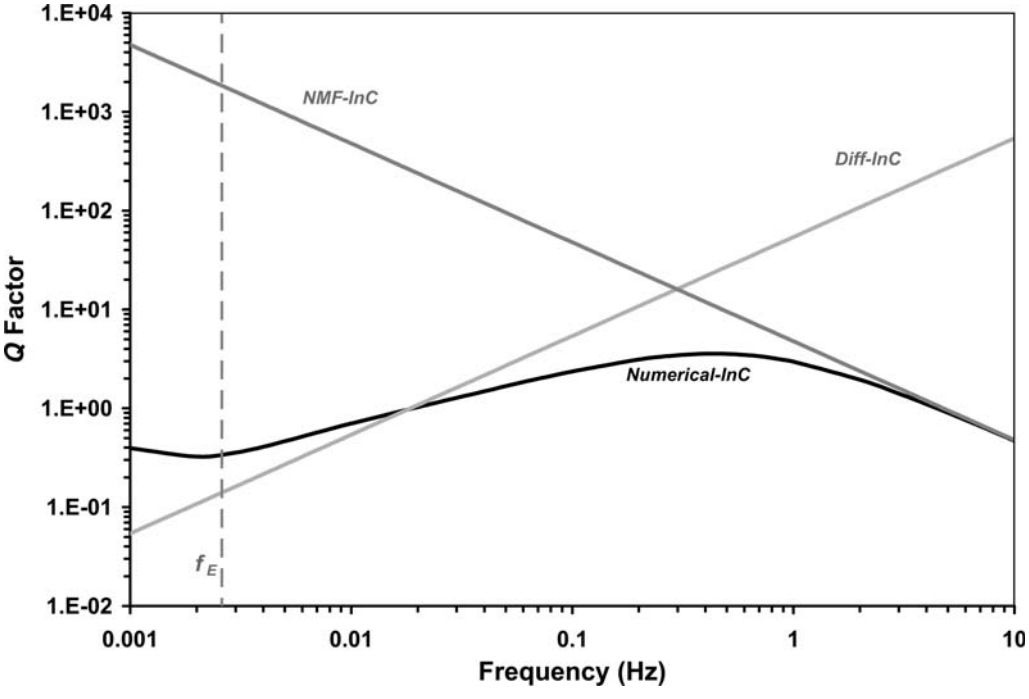

Fig. 4. The incompressible, viscous numerical solution for $Q(fr)$. The numerical solution corresponds to the incompressible analytical solutions and to f_E (see text for further explanation). *Magma properties*: $P_0 = 40$ MPa; $R_0 = 10$ μm; $D = 10^{-11}$ m^2 s^{-1}; $\eta = 10^6$ Pa · s; $n_d = 10^{12}$ m^{-3}. *Abbr: InC* – Incompressible; *Diff* – Diffusive.

solution. In the NMF solution, damping increases with increasing frequency, therefore, the numerical solution exhibits a local maximum before sticking to the NMF solution as frequency continues to increase.

The numerical solution for a visco-elastic melt

Accounting for melt compressibility requires a visco-elastic bubble growth formulation (Appendix B) and modification of the numerical code. Examination of the results emphasizes two end-member behaviours which are distinguished by their different values for the non-dimensional *Peclet* number. The *Peclet* number, *Pe*, is a measure of the relative importance of advection to diffusion. In our case, the only process controlling the NMF timescale is the viscous melt deformation, which in some sense may be viewed as an advective timescale. Therefore, the ratio between the diffusive timescale, R_0^2/D, and the NMF timescale, $\approx \eta/P_0$, could also be referred to as the *Peclet* number:

$$Pe = \frac{\tau_D}{\tau_{NMF}} = \frac{P_0 R_0^2}{D\eta}. \quad (39)$$

High *Peclet* numbers indicate that bubble growth is dominated by melt deformation expressed by the NMF approximation, while low *Peclet* numbers indicate the dominant role of volatile diffusion.

The high-Peclet *end-member.* As can be seen in Figure 5a, the incompressible assumption is valid for very low frequencies, up to f_E, the equilibrium frequency-scale. At higher frequencies, compressibility becomes more important, introducing elastic deformation to the total strain of the bubble. This effect is responsible for the larger Q values exhibited by the visco-elastic numerical solution. As frequency increases, the role of diffusion in damping is decreased and Q increases like in the diffusive analytical solution. This trend continues until diffusion becomes negligible and Q approaches the compressible NMF analytical solution. In the case of plane waves, differing from radial oscillations, the numerical solution is applicable up to the frequency where the viscous-related dissipation of the melt (Eq. A21 in Appendix A) is larger than the bubble-related dissipation. For even higher *Peclet* numbers, the approximation of NMF becomes valid at even lower frequencies than shown in Figure 5a.

The low-Peclet *end-member.* This is the case for very efficient diffusion leading to dominance of visco-elastic resistance in the nature of damping. Therefore, melt compressibility comes into consideration at lower frequencies than f_E, and the incompressible assumption is valid only for very low frequencies. So, for very low frequencies Q decreases with increasing frequency. However, as Q approaches the viscous analytical solution, it reaches a minimum (at a frequency smaller than f_E) and then increases with increasing frequency, approaching the viscous analytical solution. As shown in Figure 5b, for higher frequencies the viscous and the compressible NMF solutions converge and both are higher than the incompressible model. As in the high-*Peclet* end-member (Fig. 5a), for plane waves, the numerical solution is applicable up to the frequency where the viscous-related dissipation of the melt is larger than the bubble-related dissipation.

Discussion: the factors controlling attenuation

The roles of melt viscosity, elasticity, water diffusion, bubble size, bubble number density and the equilibrium pressure on the attenuation of pressure waves were examined by changing the parameters: η, μ, D, R_0, n_d and P_0, respectively (Table 2). We examined the *Q factor* as a function of frequency since the frequency provides the time-window for the various deformations to take place, interact and attenuate seismic waves. As magma is a compressible fluid, our coming discussion will naturally focus on the visco-elastic numerical solution.

The dependency of f_E *(the equilibrium frequency-scale) on the number density*

The equilibrium timescale, τ_E, describes the time required for diffusivity, D, to act along the diffusion length-scale, approximated by the initial shell radius, S_i. Since S_i depends on the number density, $n_d = 3/4\pi S_i^3$, it follows that low n_d leads to longer τ_E and lower f_E (the equilibrium frequency-scale which is the inverse of τ_E) (Fig. 6a). f_E is a good measure for the transition from equilibrium regime to diffusive regime for small vesicularities and negligible melt compressibility. For larger bubbles, the diffusion length-scale becomes smaller than S_i, and the transition from equilibrium regime to diffusive regime is at higher frequencies than f_E. We may assume incompressibility at high Pe values ($Pe > 1$) only if the frequencies are low enough for water transfer to take place and control deformation. For lower values of the *Peclet* number, corresponding to an efficient water transfer to and from the bubble, viscosity controls deformation, and the *Q factor* begins its approach to the viscous analytical solution at frequencies lower than f_E.

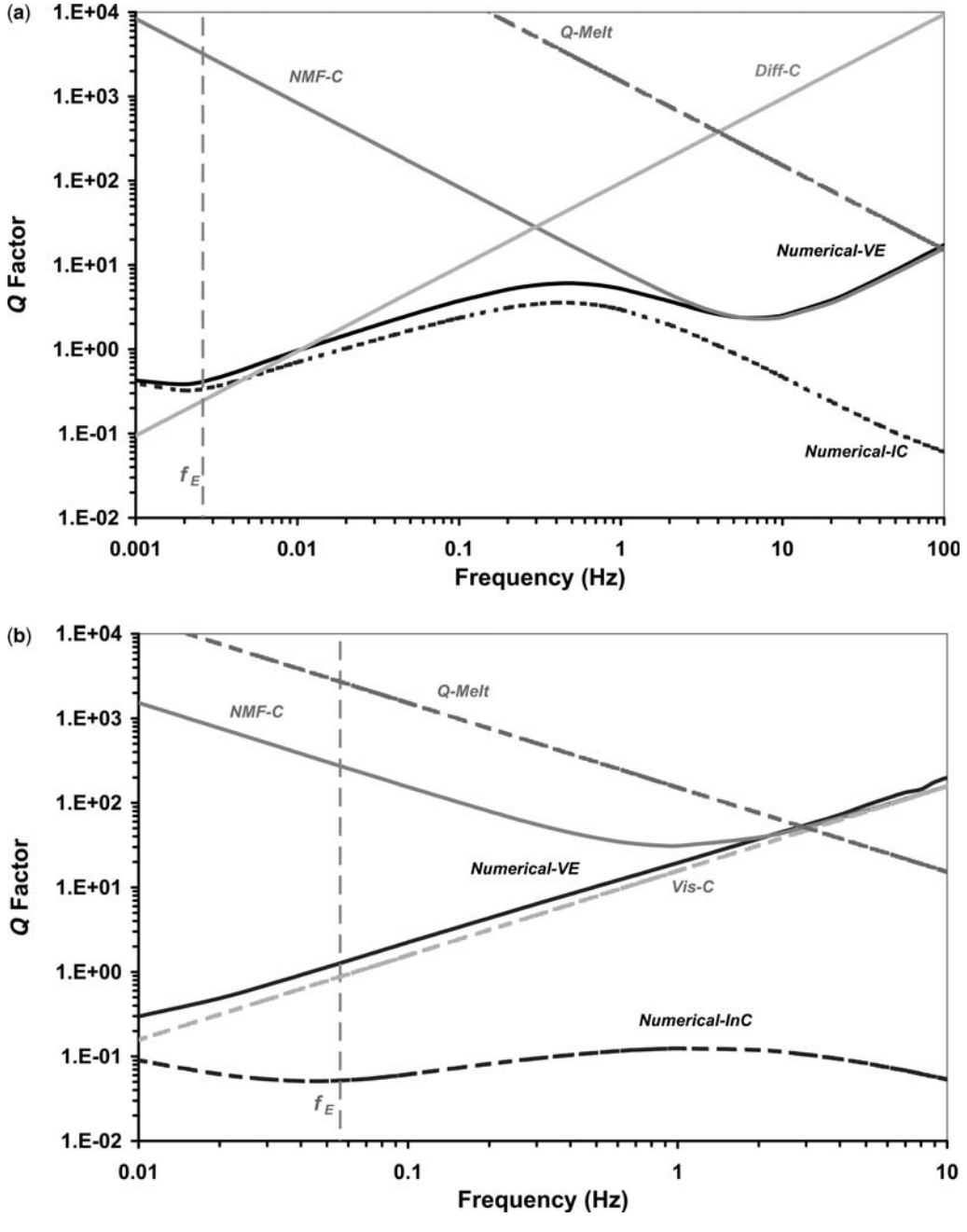

Fig. 5. The visco-elastic numerical solution for $Q(fr)$. The relations of the numerical solution to the compressible analytical solutions, the incompressible numerical solution, the viscosity-related *Q-melt* (see equation A21 in Appendix A) and f_E (see text for further explanation). (**a**) The solution for high-*Peclet* conditions. In this case, the viscous analytical solution is irrelevant. Magma properties are as in Figure 4. (**b**) The solution for low-*Peclet* conditions. In this case, the diffusive analytical solution is irrelevant. *Magma properties*: $P_0 = 80$ MPa; $R_0 = 1$ μm; $D = 10^{-11}$ m^2 s^{-1}; $\eta = 10^7$ Pa · s; $n_d = 10^{14}$ m^{-3}. *Abbr: VE* – Visco-elastic; *C* – Compressible; *InC* – Incompressible; *Diff* – Diffusive; *Vis* – Viscous.

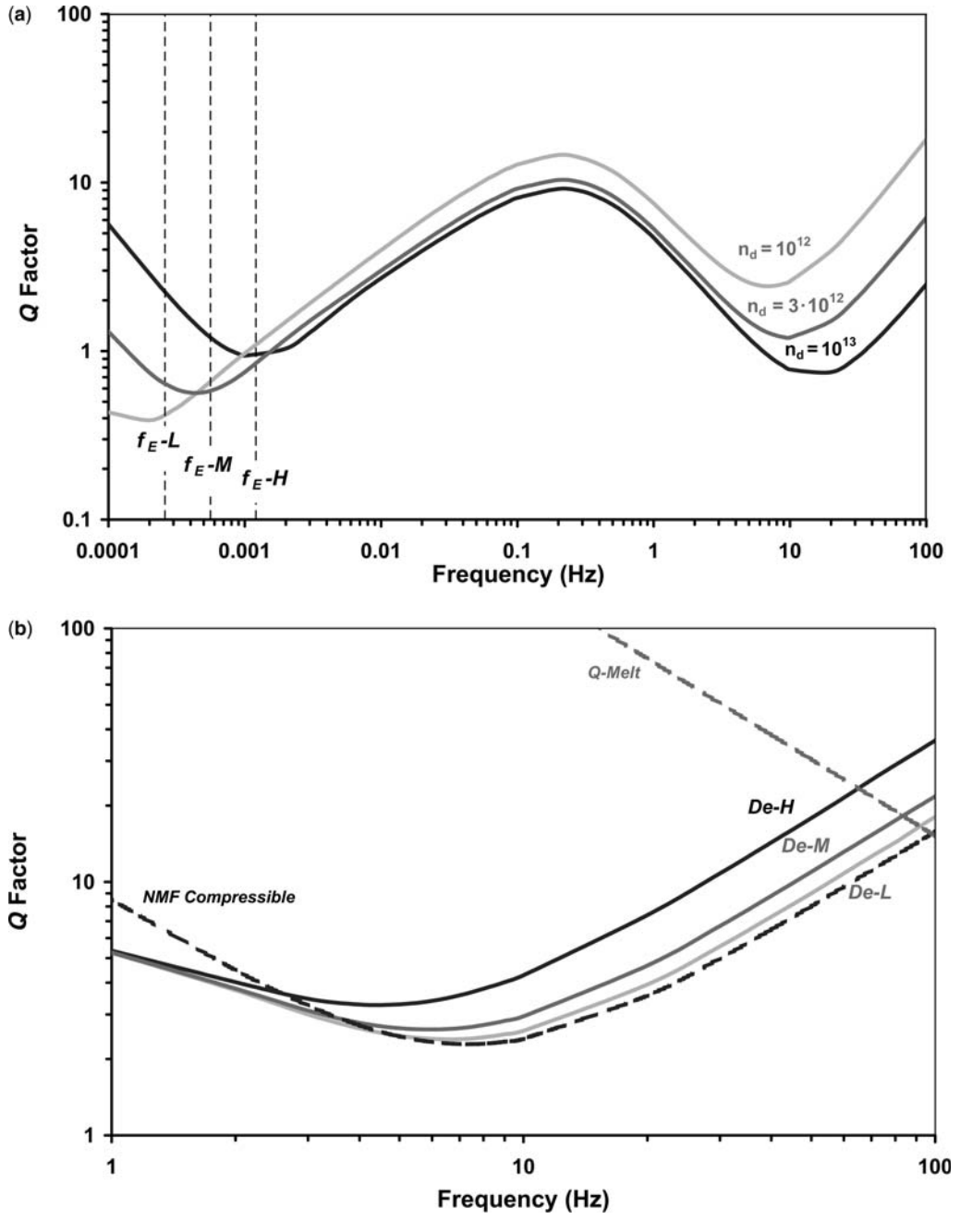

Fig. 6. (**a**) The influence of the number density, n_d, on the upper-frequency limit for reaching chemical equilibrium. For lower number densities, the shell becomes larger leading to longer times for obtaining equilibrium; hence, f_E becomes smaller. *Magma properties:* $P_0 = 40$ MPa; $R_0 = 1$ μm; $D = 10^{-12}$ m^2 s^{-1}; $\eta = 10^6$ Pa · s. (**b**) The influence of the Deborah number, *De*, on the *Q factor* for high frequencies. When the Deborah number approaches zero, elastic deformation has no influence on damping and the compressible NMF analytical solution is valid. Elastic deformation becomes important when the shear modulus of the melt is decreased, leading to an increase in *De* (see text for the full explanation). For plane-waves, the solutions are applicable up to the frequency where they intersect with the viscosity-related *Q-melt. Magma properties:* $P_0 = 40$ MPa; $R_0 = 10$ μm; $D = 10^{-11}$ m^2 s^{-1}; $\eta = 10^6$ Pa · s. *The variation in shear modulus*: *De-L:* $\mu = 1$ GPa; *De-M:* $\mu = 0.3$ GPa; *De-H:* $\mu = 0.1$ GPa. *Abbr: L* – low; *M* – moderate; *H* – high.

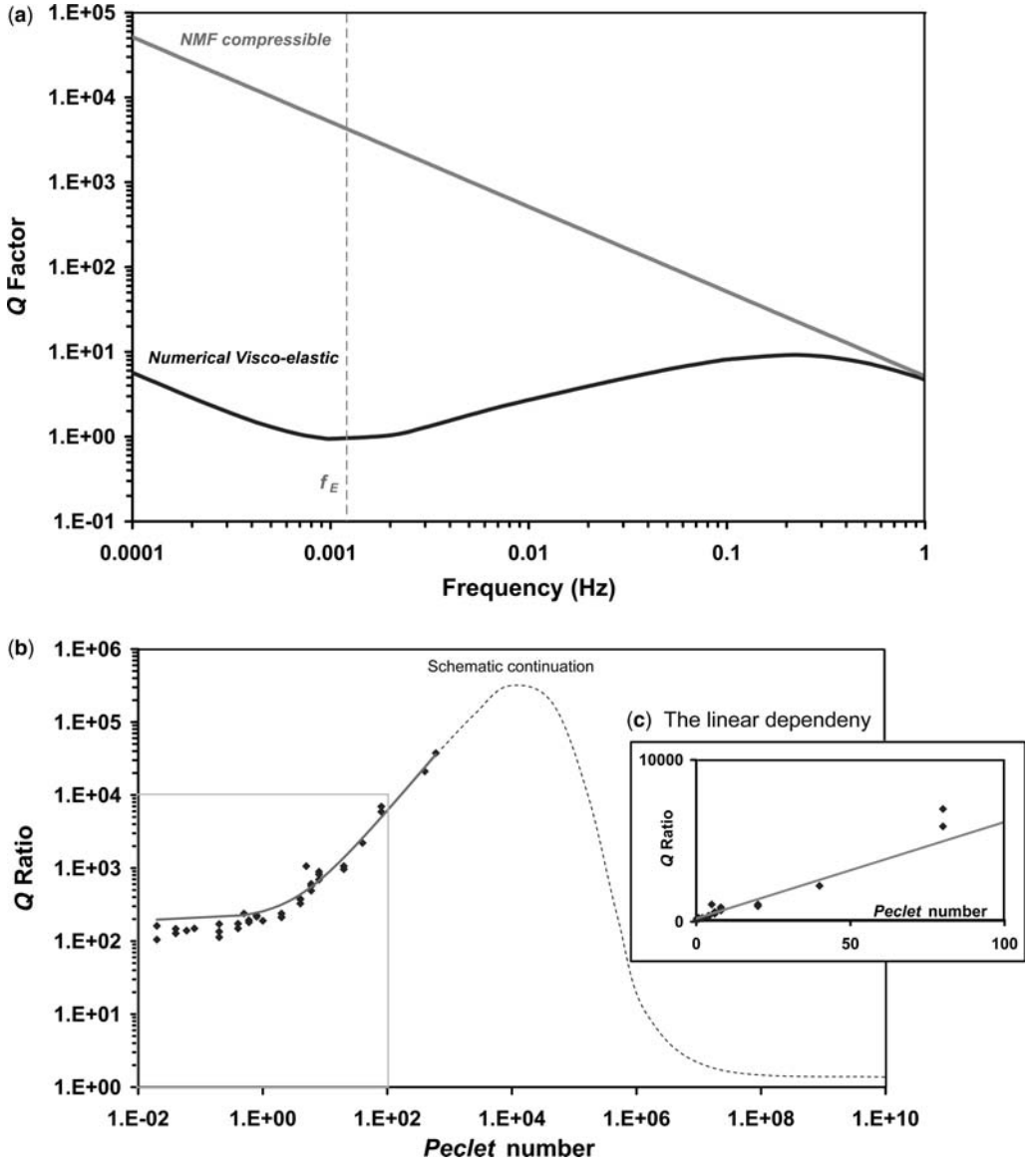

Fig. 7. The relation between the *Q factor* and the *Peclet* number for very low frequencies. (**a**) At very low frequencies, when the numerical solution is parallel to the NMF solution, we may produce a *Q ratio* defined as Q_{NMF}: $Q_{Numerical}$. (**b**) Plotting this ratio against the *Peclet* number (keeping n_d and μ constant), we obtain an interesting relation. The *Q ratio* is linear with the *Peclet* number for $Pe < 1000$ (the axes are in log scale). Beyond $Pe \approx 1000$, the *Q ratio* increases non-linearly with *Pe*, reaching a maximum and descends towards a value of 1 *as the numerical solution approaches the NMF solution.* (**c**) An enlargement of the linear section up to $Pe = 10$, showing the intersection with the *Q ratio* axis for very low values of *Pe*. This intersection provides a constant, representing the basic increase in damping as mass transfer is introduced into the system. *Here,* $n_d = 10^{15}$ m^{-3} and $\mu = 1$ GPa.

The role of elastic deformation

The shear modulus of silicic magmas at high temperatures is not well constrained. Experimental studies (Dingwell 1998) for very viscous silicic magmas show that Maxwell relaxation time does not exceed 0.01 seconds. We expect that for $\omega \approx 100$ Hz the *Deborah* number ($De = \eta/\mu\omega$) approaches one ($De \to 1$), and elasticity will take a larger role in the total deformation of the melt.

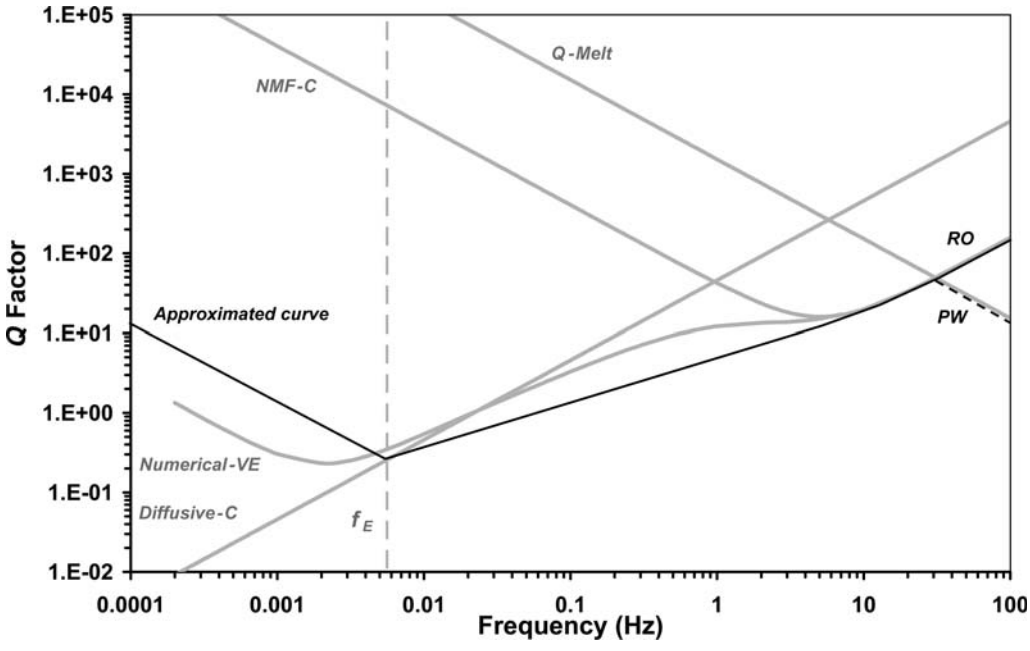

Fig. 8. The approximation of the numerical solution for Q when $1 < Pe < 1000$. Up to f_E, $Q \propto 1/\omega$ and runs parallel to the NMF solution, but is displaced to lower Q values according to the *Peclet* number. Beyond f_E, the Q curve ascends with increasing frequency, gradually approaching the compressible NMF solution (equation 24).
Abbr: C – Compressible; *VE* – Visco-elastic; *PW* – Plane Waves; *RO* – Radial Oscillations.

This effect is shown in Figure 6b, where it is shown that as *De* increases, Q increases, and damping decreases.

In this case, the increase of *De* is done by decreasing the shear modulus (keeping all the other parameters constant). This, in fact, conceals a very interesting effect: reducing μ indicates weakening of the elastic components of the melt, which allows a larger elastic deformation to be taken by the melt; this may occur in hydrous, vesicular magmas ($\mu \approx 10^6$ Pa according to Mungall *et al.* 1996, Romano *et al.* 1996 and Dingwell 1998) leading to even higher Q values than the ones presented in Figure 6b.

Attenuation at very low frequencies

The *Peclet* number is also important for the understanding of damping at very low frequencies. At these low frequencies, the numerical solution is proportional to $1/\omega$, exactly like in the NMF analytical solution, differing only by a factor (Fig. 7a). This means that the addition of diffusion into the system can be accounted for by dividing the NMF solution by a factor. We found that this factor corresponds to the *Peclet* number. For a constant number density and for $Pe < 1000$, we found that the Q *ratio*, $Q_{NMF}/Q_{Numerical}$, increases linearly with increasing *Peclet* numbers (Fig. 7b). Thus, for very low *Peclet* numbers, corresponding to a very efficient diffusion, the addition of diffusion is responsible for a fixed increase in damping (the intersection with the Q *ratio* axis in the enlargement — Fig. 7c).

Higher *Peclet* numbers mean that the diffusion process becomes less efficient and chemical equilibrium is harder to obtain. This leads to an increase in the actual damping, which means that $Q_{Numerical}$ decreases, leading to an increase in the Q *ratio*. On the other hand, very high *Peclet* numbers ($Pe \gg 1000$) mean that the NMF approximation is valid and therefore, $Q_{ratio} \to 1$. So as the *Peclet* number increases, the increase in the Q *ratio* reaches a maximum before decreasing into the NMF approximation (Figmm. 7b).

Analytical approximation for the visco-elastic numerical solution

For $De < 1$, we present a simple scheme for approximating analytically the Q *factor* according to the *Peclet* number of the system. For very high *Peclet* numbers (see Fig. 7b), we may approximate the Q

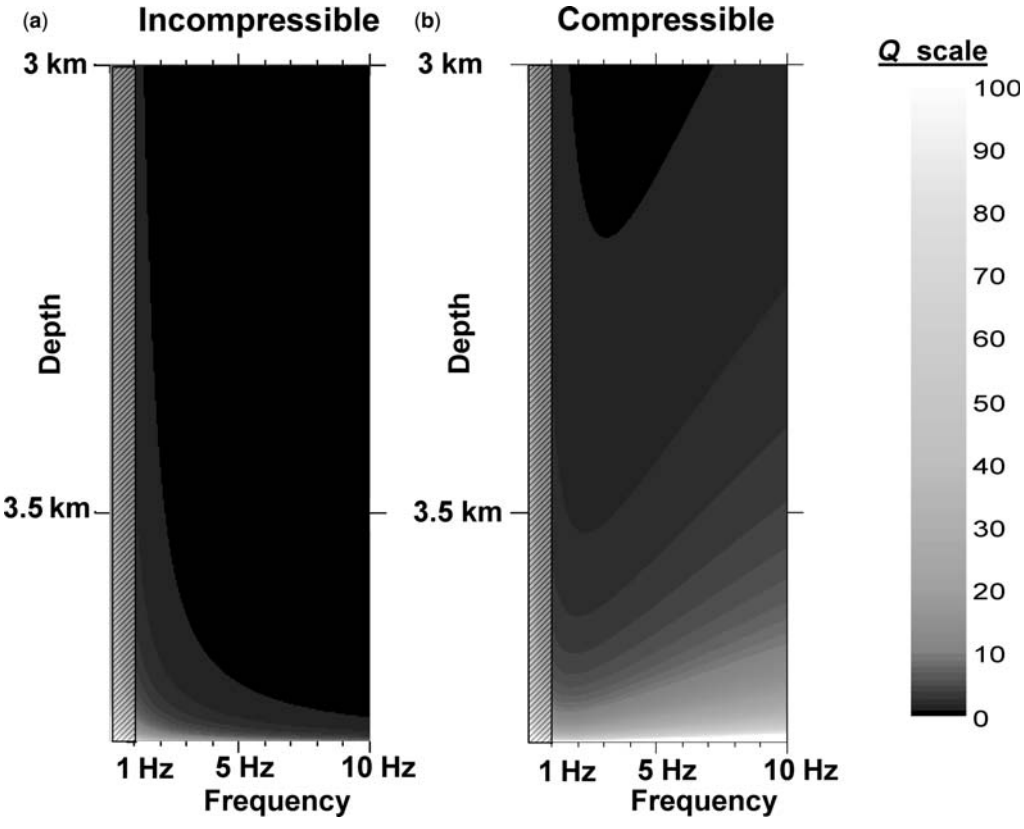

Fig. 9. The *Q(f, depth)* conduit profiles for NMF conditions. We present a comparison between an incompressible profile (following Collier *et al.* 2006) and a visco-elastic profile, accounting also for melt compressibility. The dashed area for $f < 1$ Hz indicates that both profiles are a close approximation to their corresponding numerical solution only from *c.* 1 Hz and higher. The addition of compressibility leads to very different profiles than the ones presented in Collier *et al.* (2006). Here, we present the lower section of the conduit where compressibility has a major role in the damping properties of the magma. *Magma properties:* $P_0 = 125$ MPa; $D = 2 \cdot 10^{-11}$ m^2 s^{-1}; $\eta = 10^7$ Pa · s; $n_d = 10^{12}$ m^{-3}; Initial water concentration = 4.6%.

factor using the compressible NMF analytical solution (equation 24).

$10^3 > \mathrm{Pe} > 1$ — Up to f_E, $Q \propto 1/\omega$ and runs parallel to the NMF solution, but is displaced to lower Q values according to the *Peclet* number. Beyond f_E, the Q curve ascends with increasing frequency, gradually approaching the compressible NMF solution (equation 24; Fig. 8).

$Pe < \approx 1$ — At very low frequencies, $Q \propto 1/\omega$ according to a $Q_{NMF}/Q_{Numerical}$ ratio that can be approximated by statistical curve fitting. At higher frequencies, the numerical solutions for Q fall close to the viscous analytical solution (equation 30), they gradually approach it and Q increases with increasing frequency.

For plane waves, as opposed to radial oscillations (Fig. 8), the *Q factor* will decrease beyond the frequency where the viscous-related dissipation of the melt is larger than the bubble-related dissipation (see Eq. A21 in Appendix A).

The Q(f) *depth-profile*

Applying our model to a magma-filled conduit, we produced a $Q(f)$ depth-profile and compared it to the one presented by Collier *et al.* (2006). We find a major difference between the $Q(f)$ profile they obtained (see Figure 9 in Collier *et al.* 2006) and the $Q(f)$ profile obtained here (Fig. 9). While their profile shows that Q decreases with increasing frequency, simply following the incompressible NMF solution, our profile shows an opposite behaviour: the addition of melt compressibility leads to an increase in Q for increasing frequency. Our

results indicate larger values of the visco-elastic Q, which become important in the lower section of the conduit. For frequencies of *c.* 1 Hz and above, we find that similar to Collier *et al.* (2006), showing that the incompressible NMF solution closely approximates the incompressible numerical solution, we show that in our profile the compressible NMF solution closely approximates the visco-elastic numerical solution.

This may be significant for low-frequency earthquakes (LFs). These volcanic earthquakes originate at the vicinity of the magma conduit, and are regarded as an important indicator prior to explosive eruptions (Neuberg *et al.* 2000). Their typical waveform is a narrowband signal presenting an initial stage of amplification followed by a long tail of attenuation. This signature reflects excitation in a resonating system (Chouet 1996). Two main approaches were advanced for explaining the resonating system: the fluid-filled crack resonator (Aki *et al.* 1977; Chouet 1986, 1988) and the magma-filled conduit resonator (Neuberg *et al.* 2000). In the case of a magma-filled conduit, pressure waves propagating through the bubbly magma are expected to be attenuated, resulting in an ineffective conduit resonator. According to Collier *et al.* (2006), there is a very limited depth-range where the Q values are high enough to allow efficient wave propagation in the bubbly magma. The present findings extend this depth-range, improving significantly the efficiency of the magma-filled conduit as a possible resonator of low-frequency earthquakes. Following decompression, magma may become supersaturated, leading to an accelerated bubble growth and releasing additional energy into the system. This energy may be partly converted into seismic energy, reducing damping or even leading to wave-amplification.

Conclusions

Based on the theoretical approach of Commander & Prosperetti (1989), we have developed a theory for damping of pressure waves in saturated bubbly magma and obtained analytical and numerical solutions. We have shown that the analytical end-member solutions are related to the incompressible and visco-elastic numerical solutions, and allow better understanding of physical processes controlling wave attenuation under various magma properties.

Furthermore, we found out that the dynamic behaviour of pressure waves propagating in bubbly magma can be obtained by the compressible NMF solution combined with the following three characteristic magma properties: (i) the *Peclet* number, defining the ratio between the diffusive and NMF timescales; (ii) the *Deborah* number, defining the visco-elastic nature of the melt; and (iii) the number density of bubbles in the melt.

We demonstrated analytically and numerically the dominant role of compressibility in reducing the attenuation of pressure waves; this role becomes even more significant for high frequencies (≥ 1 Hz). Applying our model to a magma-filled conduit, we demonstrated that the compressible NMF solution is apparently a good approximation for a wide range of natural conditions, and that it improves the resonating qualities of a magma-filled conduit.

We thank Jurgen Neuberg for useful discussions, the reviewers: Mie Ichihara and Dork Sahagian for constructive reviews, and the editors: Steve Lane and Jennie Gilbert. I. Kurzon thanks Amotz Agnon and Yizhaq Makovsky for giving advice and suggestions. Funding was provided by the EC MULTIMO project and by the USA–Israel Binational Science Foundation (grant 2004046).

Appendix A. The formulation of Commander & Prosperetti (1989)

The formulation of Commander & Prosperetti (1989) is based on the theory of Van Wijngaarden (1968). Here, we obtain their equation (1) starting with the equation of motion (Newton's 2nd law):

$$\rho \frac{\partial^2 u_i}{\partial t^2} = \frac{\partial \sigma_{ij}}{\partial x_j} \tag{A1}$$

where ρ is the density of the suspension, u_i is the total displacement and σ_{ij} is the stress tensor. By taking the divergence of (A1) and changing the order of derivatives, we get:

$$\rho \frac{\partial^2}{\partial t^2}\left(\frac{\partial u_i}{\partial x_i}\right) = \frac{\partial^2 \sigma_{ij}}{\partial x_i \partial x_j}. \tag{A2}$$

The total volume of the magma is a sum of melt and gas volumes. Hence, the total volumetric deformation $(\partial u_i/\partial x_i)$ is a sum of two components:

$$\frac{\partial u_i}{\partial x_i} = \frac{\partial u_i^{(m)}}{\partial x_i} + \phi. \tag{A3}$$

The first term $(\partial u_i^{(m)}/\partial x_i)$ corresponds to the melt compaction, and the second one to the change in vesicularity (relative to some background value). Compaction of the melt is proportional to the pressure, P:

$$\frac{\partial u_i^{(m)}}{\partial x_i} = -\frac{P}{K} \tag{A4}$$

where K is the bulk modulus of the melt. Finally, the volumetric deformation results in:

$$\frac{\partial u_i}{\partial x_i} = \frac{-P}{K} + \phi. \tag{A5}$$

The stress tensor could also be separated into volumetric (mean stress or pressure) and deviatoric components:

$$\sigma_{ij} = \frac{1}{3}\sigma_{nn}\delta_{ij} + \tau_{ij} = -P\delta_{ij} + \tau_{ij}. \quad \text{(A6)}$$

For small vesicularity, the melt pressure used in (A5) is equal to the ambient pressure, on the outer boundary of the shell, used in (A6). The second derivative of the stress tensor is:

$$\frac{\partial^2\sigma_{ij}}{\partial x_i \partial x_j} = -\nabla^2 P + \frac{\partial^2\tau_{ij}}{\partial x_i \partial x_j} = -\nabla^2 P + H \quad \text{(A7)}$$

where H is a scalar variable used for notation. Substituting (A5) and (A7) back into (A2) yields:

$$\frac{\rho}{K}\frac{\partial^2 P}{\partial t^2} - \nabla^2 P + H = \rho\frac{\partial^2\phi}{\partial t^2}. \quad \text{(A8)}$$

Neglecting the term H related to the deviatoric stress and using the notation $c^2 = K/\rho$ for the speed of sound, we end up with the following wave equation:

$$\frac{1}{c^2}\frac{\partial^2 P}{\partial t^2} - \nabla^2 P = \rho\frac{\partial^2\phi}{\partial t^2}. \quad \text{(A9)}$$

For small vesicularities ($\phi \ll 1$), we can approximate $\rho \approx \rho_m$ (where ρ_m is the melt density) and c is the speed of sound in the melt. These approximations lead to equation (1), the wave equation obtained by Van Wingaarden (1968), which is applied in our model. For $\partial^2\phi/\partial t^2 = 0$, (A9) reduces to a linear wave equation for a non-dissipative medium.

Now we derive the conditions that allow neglecting the deviatoric stress (dropping H from equation 8). Following Maxwell's visco-elastic model, the total deviatoric strain rate, e_{ij}, is a sum of elastic and viscous components:

$$e_{ij} = \frac{1}{2\mu}\frac{\partial\tau_{ij}}{\partial t} + \frac{\tau_{ij}}{2\eta} \quad \text{(A10)}$$

where μ and η are the effective shear modulus and viscosity of the porous melt. Assuming small void fraction and deformable bubbles, we may use Mackenzie's expression $\eta = \eta_o\ (1 - 5\alpha/3)$, $\mu = \mu_o\ (1 - 5\alpha/3)$ (Ichihara & Kameda 2004).

Taking the second derivative yields:

$$\frac{\partial^2 e_{ij}}{\partial x_i \partial x_j} = \frac{1}{2\mu}\frac{\partial H}{\partial t} + \frac{H}{2\eta}. \quad \text{(A11)}$$

Using the definition for the strain rate

$$e_{ij} = \frac{1}{2}\frac{\partial}{\partial t}\left(\frac{\partial u_i}{\partial x_j} + \frac{\partial u_j}{\partial x_i} - \frac{2}{3}\cdot\frac{\partial u_n}{\partial x_n}\delta_{ij}\right) \quad \text{(A12)}$$

and taking its second derivative leads to

$$\frac{\partial^2 e_{ij}}{\partial x_i \partial x_j} = \frac{2}{3}\nabla^2\left(\frac{\partial}{\partial t}\left(\frac{\partial u_n}{\partial x_n}\right)\right). \quad \text{(A13)}$$

Substituting (A5) into (A13) and then into (A11) yields

$$\frac{1}{2\mu}\frac{\partial H}{\partial t} + \frac{H}{2\eta} = \frac{2}{3}\nabla^2\left(\frac{\partial}{\partial t}\left(-\frac{P}{K} + \phi\right)\right). \quad \text{(A14)}$$

The H-value obtained from (A14) should be incorporated in (A8) to account for the effect of the deviatoric stress components propagation of P-waves. Comparing the first and the second term on the left-hand side of (A14), we discuss two end-member cases: (a) $\omega/2\mu \gg 1/2\eta$ corresponding to negligible role of the viscous strain components and (b) $\omega/2\mu \ll 1/2\eta$, corresponding to negligible role of the elastic strain components.

In the first case, H is equal to

$$H = \frac{4}{3}\mu\nabla^2\left(-\frac{P}{K} + \phi\right) \quad \text{(A15)}$$

leading to two extra terms in the wave equation (A8):

$$\frac{\rho}{K}\frac{\partial^2 P}{\partial t^2} - \nabla^2 P - \frac{4}{3}\frac{\mu}{K}\nabla^2 P + \frac{4}{3}\mu\nabla^2\phi = \rho\frac{\partial^2\phi}{\partial t^2}. \quad \text{(A16)}$$

The additional term of $\nabla^2 P$ leads to a well-known expression for p-wave velocity in an elastic media ($\rho\ V_p^2 = K + 4/3\mu$). The ratio between the second term and the first term of $\nabla^2 P$ gives: $4\mu/3K$. The second, vesicularity-related term is of the order of $\mu\phi L^2$ (where L is the wavelength), which should be compared with the right-hand-side term, of the order of $\rho\phi\omega^2$ (where ω is the angular frequency). Using $L^2\omega^2 = V_p^2 \approx K/\rho$, the ratio between these two terms is also $4\mu/3K$, which is generally lower than one for magmas, and may get very low for hydrous, silicate melts ($\mu \approx 10^6$ Pa according to Mungall *et al.* 1996; Romano *et al.* 1996; Dingwell 1998, while $K \approx 10^{10}$ Pa). Hence, the elastic components in the deviatoric stresses can be ignored, leading to equation A9.

In the second case ($\omega/2\mu \ll 1/2\eta$), the elastic components are neglected, resulting in

$$H = \frac{4}{3}\eta\nabla^2\left(\frac{\partial}{\partial t}\left(-\frac{P}{K} + \phi\right)\right) \quad \text{(A17)}$$

which lead to two additional terms in the wave equation (A8):

$$\frac{\rho}{K}\frac{\partial^2 P}{\partial t^2} - \nabla^2 P - \frac{4}{3}\frac{\eta}{K}\frac{\partial}{\partial t}\left(\nabla^2 P\right) + \frac{4}{3}\eta\frac{\partial}{\partial t}\left(\nabla^2\phi\right) = \rho\frac{\partial^2\phi}{\partial t^2}. \quad \text{(A18)}$$

For $\phi = 0$, we may solve (A18), and obtain the role of melt viscosity in wave attenuation. Applying $\delta P(x, t) = A\exp(ikx - i\omega t)$, we obtain

$$-\frac{\omega^2}{c^2} + k^2 = i\frac{4}{3}\frac{\eta}{K}\omega k^2 \tag{A19}$$

which for $\omega = kV$ may be re-organized as:

$$V^2 = c^2\left[1 - \frac{4\eta\omega}{3K}i\right]. \tag{A20}$$

Substituting (A20) into the definition of Q (equation 6), we obtain

$$Q = \frac{3K}{4\eta\omega}. \tag{A21}$$

This equation describes the melt-related Q, which for propagating plane-waves provides the upper frequency-limit of our model (see Figures 5, 6b and 8). The additional vesicularity-related term is of the order of $\eta\phi\omega/L^2$, while the right hand-side term, as in the previous elastic case, is of the order of $\rho\phi\omega^2$; their ratio is $4\eta\omega/3K$.

This means that in order to neglect the viscosity-related terms and to use equation A9, we require that $4\eta\omega/3\mathrm{K} \ll 1$ and that the melt-related Q is higher than the bubble-related Q. For $K \approx 10^{10}$ and $\eta \approx 10^6$, the frequency of the pressure waves cannot exceed 100 Hz, and for $\eta \approx 10^7$ it cannot exceed 10 Hz.

Appendix B. The visco-elastic bubble growth model

Strain–stress relationship

We use Maxwell visco-elastic model that assumes superposition of deformations associated with different mechanisms. This assumption is expressed as

$$\varepsilon_{ij}^{tot} = \varepsilon_{ij}^{el} + \varepsilon_{ij}^{vis} \tag{B1}$$

where ε_{ij}^{tot} is the total strain, ε_{ij}^{vis} is the viscous strain and ε_{ij}^{el} is the elastic strain. The total Cauchi strain tensor, ε_{ij}^{tot}, is related to the displacement, u_i by

$$\varepsilon_{ij}^{tot} = \frac{1}{2}\left(\frac{\partial u_i}{\partial x_j} + \frac{\partial u_j}{\partial x_i}\right). \tag{B2}$$

The elastic strain tensor is related to the stress tensor, σ_{ij}^{el}, through Hooke's law:

$$\sigma_{ij} = \lambda\varepsilon_{kk}^{el}\delta_{ij} + 2\mu\varepsilon_{ij}^{el} \tag{B3}$$

where λ and μ are Lame coefficients (and μ is also known as the shear modulus or the rigidity), and δ_{ij} is the unit tensor (Einstein summation convention is used).

The stress tensor could be represented as the sum of volumetric stress (diagonal components) and deviatoric stress. The pressure is equal to

$$P = -\frac{\sigma_{\alpha\alpha}}{3} = -\left(\lambda + \frac{2}{3}\mu\right)\varepsilon_{\alpha\alpha}^{el} \tag{B4}$$

where $\sigma_{\alpha\alpha}$ is the sum of volumetric stress components and $\varepsilon_{\alpha\alpha}^{el}$ is the sum of the elastic strain components. By using the definitions $\varepsilon_{\alpha\alpha}^{el} = div(u_i)$ for the sum of the volumetric strain components and $K = \lambda + \frac{2}{3}\mu$ for the bulk modulus, we may re-express (B4) as:

$$P = -K \cdot div(u_i) \tag{B5}$$

Similarly, the deviatoric stresses $\tau_{ij} = \sigma_{ij} - \frac{1}{3}\sigma_{\alpha\alpha}\delta_{ij}$ and the deviatoric strains $\tilde{\varepsilon}_{ij}^{el} = \varepsilon_{ij}^{el} - \frac{1}{3}\varepsilon_{\alpha\alpha}^{el}\delta_{ij}$ are proportional:

$$\tau_{ij} = 2\mu\tilde{\varepsilon}_{ij}^{el}. \tag{B6}$$

The rate of viscous strain accumulation in Newotonian media with viscosity, η, is:

$$\frac{d\tilde{\varepsilon}_{ij}^{vis}}{dt} = \frac{1}{2\eta}\tau_{ij}. \tag{B7}$$

Substituting (B6) and (B7) back into (B1) yields $\tilde{e}_{ij}$, the total deviatoric strain rate tensor:

$$\tilde{e}_{ij} \equiv \frac{d\tilde{\varepsilon}_{ij}^{tot}}{dt} = \frac{\tau_{ij}}{2\eta} + \frac{\dot{\tau}_{ij}}{2\mu}. \tag{B8}$$

The ratio between the elastic and viscous terms in (B8) provides the non-dimensional *Deborah* number discussed earlier in this paper.

For constant shear coefficients, μ and η, the general solution of (B8) is

$$\tau_{ij}(t) = \exp\left(-\frac{t}{\tau_m}\right)\left[\int 2\mu\tilde{e}_{ij}\exp\left(\frac{t}{\tau_m}\right)dt + \tau_0\right] \tag{B9}$$

where $\tau_m = \eta/\mu$ is the Maxwell relaxation time and τ_0 is the stress at $t = 0$.

3-D spherical symmetry

Assuming 3-D spherical symmetry, we search a solution for radial displacement $u_r(r, t)$ as a function of the distance, r, from the centre of the bubble and time, t, with no tangential components of the displacement:

$$u_r(r) = a(t)r + \frac{b(t)}{r^2}. \tag{B10}$$

Therefore, the components of the strain tensor in spherical coordinates are:

$$\varepsilon_{rr}(r) = \frac{\partial u_r}{\partial r} = a(t) - \frac{2b(t)}{r^3}$$
$$\varepsilon_{\theta\theta}(r) = \varepsilon_{\phi\phi}(r) = \frac{u_r}{r} = a(t) + \frac{b(t)}{r^3} \tag{B11a, b}$$

and the radial velocity is

$$v_r(r) = \dot{a}(t)r + \frac{\dot{b}(t)}{r^2}. \tag{B12}$$

For $\dot{b}(t) = v_R R^2$ and $a(t) = const$, (B12) reduces to the radial distribution of melt velocity in an incompressible viscous fluid:

$$v_r(r) = v_R \frac{R^2}{r^2}. \tag{B13}$$

We may separate the strain tensor to deviatoric and volumetric components resulting in

$$\begin{aligned} \tilde{\varepsilon}_{rr} &= -\frac{2b(t)}{r^3} \\ \tilde{\varepsilon}_{\theta\theta} &= \tilde{\varepsilon}_{\phi\phi} = \frac{b(t)}{r^3} \\ div(u_i) &\equiv \varepsilon_{\alpha\alpha} = 3a(t) \end{aligned} \tag{B14a–c}$$

leading to the following shear strain rates

$$\begin{aligned} e_{rr} &\equiv \dot{\varepsilon}_{rr}(r) = -\frac{2\dot{b}(t)}{r^3} \\ e_{\theta\theta} &= e_{\phi\phi} \equiv \dot{\varepsilon}_{\theta\theta}(r) = \dot{\varepsilon}_{\phi\phi}(r) = \frac{\dot{b}(t)}{r^3}. \end{aligned} \tag{B15a,b}$$

Substitution of (B14c) into (B5) and of (B15a, b) into (B9) results with the following stresses:

$$\begin{aligned} P &= -3Ka(t) \\ \tau_{rr} &= \exp\left(-\frac{t}{\tau_m}\right)\left[\int_0^t \left((-2\mu\frac{2\dot{b}(t)}{r^3})\exp\left(\frac{t}{\tau_m}\right)\right)dt + \tau_{rr}^0\right] \\ \tau_{\theta\theta} &= \tau_{\phi\phi} = \exp\left(-\frac{t}{\tau_m}\right)\left[\int_0^t \left(2\mu\frac{\dot{b}(t)}{r^3}\exp\left(\frac{t}{\tau_m}\right)\right)dt + \tau_{\theta\theta}^0\right]. \end{aligned} \tag{B16a–c}$$

The time-dependent functions $a(t)$ and $b(t)$ could be found from the boundary conditions on the outer boundary of the shell ($r = S$):

$$(-P + \tau_{rr})\big|_{r=S} = -P_a \tag{B17}$$

and on the bubble-melt interface ($r = R$):

$$(-P + \tau_{rr})\big|_{r=R} = -P_g + \frac{2\gamma}{R} \tag{B18}$$

where P_a is the ambient pressure acting on the outer shell, and P_g is the gas pressure in the bubble. The term $2\gamma/R$ stands for the Laplace surface tension.

Substitution of the expressions for the pressure (B16a) and for the radial stress (B16b) into the two boundary conditions results in

$$3Ka - \exp\left(-\frac{t}{\tau_m}\right)\left[\int_0^t 4\mu\frac{\dot{b}(t)}{r^3}\exp\left(\frac{t}{\tau_m}\right)dt + \tau_{rr}^0(r)\right]\Bigg|_{r=S} = -P_a \tag{B19}$$

$$3Ka - \exp\left(-\frac{t}{\tau_m}\right)\left[\int_0^t 4\mu\frac{\dot{b}(t)}{r^3}\exp\left(\frac{t}{\tau_m}\right)dt + \tau_{rr}^0(r)\right]\Bigg|_{r=R} = -P_g + \frac{2\gamma}{R}. \tag{B20}$$

Assuming that the system is in equilibrium at $t = 0$, thus $\tau_{rr}^0 \equiv 0$, and ignoring surface tension, we may re-express the boundary conditions as

$$\begin{cases} 3Ka - \dfrac{4\mu}{S^3}\exp\left(-\dfrac{t}{\tau_m}\right)\displaystyle\int_0^t \dot{b}(t)\exp\left(\frac{t}{\tau_m}\right)dt = -P_a \\ 3Ka - \dfrac{4\mu}{R^3}\exp\left(-\dfrac{t}{\tau_m}\right)\displaystyle\int_0^t \dot{b}(t)\exp\left(\frac{t}{\tau_m}\right)dt = -P_g \end{cases} \tag{B21a,b}$$

By multiplying (B21a) by S^3 and (B21b) by R^3, subtracting (B21a) from (B21b) and rearranging, we obtain the following expression for $a(t)$:

$$\begin{aligned} a(t) &= \frac{R^3P_g - S^3P_a}{3K(S^3 - R^3)} \\ &= -\frac{P_a}{3K} + \frac{1}{3K}\cdot\frac{R^3}{S^3 - R^3}(P_g - P_a). \end{aligned} \tag{B22}$$

By subtracting (B21a) from (B21b), differentiation with respect to time and dividing by the common factor, $\exp(t/\tau_m)$ we get

$$\dot{b}(t) = \dot{f}(t) + \frac{1}{\tau_m}f(t) \tag{B23}$$

where $$f(t) = \frac{P_g - P_a}{4\mu} * \frac{R^3S^3}{S^3 - R^3}.$$

Instead of calculating the radial velocity using (16) from the viscous bubble growth model, we can now calculate it according to (B12), where $\dot{a}(t)$ and $\dot{b}(t)$ are taken from (B22) and (B23); the result is given by the following equation:

$$\begin{aligned} v_r(r) = &\frac{d}{dt}\left(\frac{R^3P_g - S^3P_a}{3K(S^3 - R^3)}\right)\cdot r + \frac{1}{r^2} \\ &\times\left\{\frac{R^3S^3}{4\mu(S^3 - R^3)}\left[\frac{d}{dt}(P_g - P_a) + \frac{1}{\tau_m}(P_g - P_a)\right]\right\}. \end{aligned} \tag{B24}$$

Equation B24 couples the viscous and elastic deformations of the melt surrounding the deforming bubble. This is the equation used in the visco-elastic numerical solution for $Q(\omega)$. For an infinite shell model, this

monster (B24) gets a more elegant form:

$$v_r(r) = r \cdot \left[\frac{1}{4\eta}\left(P_g(t) - P_a(t)\right) + \frac{1}{4\mu}\frac{d\left(P_g(t) - P_a(t)\right)}{dt} - \frac{1}{3K}\frac{dP_a(t)}{dt} \right] \quad \text{(B25)}$$

and on the bubble-melt interface it yields equation 18.

Appendix C. The finite shell model

We generalized our analytical solutions to the finite shell model, where the bubble 'sees' the far boundary of the shell. However, we still keep to small oscillations and $\delta R \ll R_0$.

For the NMF solution, we should multiply τ_{NMF} by a factor of $1 + R_0^3/S_i^3$ leading to

$$Q = \frac{\eta\omega}{\rho_m \pi n_d R_0^3 c^2} \cdot \frac{S_i^3}{R_0^3 + S_i^3} + \frac{1}{\omega} \cdot \left[\frac{9P_0^2}{\rho_m 16\eta\pi n_d R_0^3 c^2} + \frac{3P_0}{4\eta} \right] \cdot \left[1 + \frac{R_0^3}{S_i^3} \right]. \quad \text{(C1)}$$

For the viscous solution, we get:

$$Q = \frac{\eta\omega}{\rho_m \pi n_d R_0^3 c^2} \cdot \frac{S_i^3}{R_0^3 + S_i^3}. \quad \text{(C2)}$$

For the diffusive solution, we use the concentration gradient definition given by Lyakhovsky *et al.* (1996) for a finite shell model:

$$\left(\frac{\partial C}{\partial r}\right)_R = \frac{S_i^3(C_0 - C_R) - \frac{\rho_g}{\rho_m}R^3}{S_i^3 R - 1.5(S^2 - R^2)R^2} \quad \text{(C3)}$$

which for $R \ll S$ reduces to (14) and converges with the infinite shell model, discussed above. Using (C3) in the development of the diffusive solution, we obtain an expression for $Q(\omega)$ that is similar to (35) but is divided by a factor of

$$F_{diff} = \frac{S_i^3}{\left\{ S_i^3 - 1.5\left[\left(S_i^3 + R_0^3\right)^{2/3} - R_0^2 \right] R_0 \right\}}. \quad \text{(C4)}$$

However, the corrections for the finite shell case are relevant only for the upper limit of the vesicularity-range considered in our model.

References

AKI, K., FEHLER, M. & DAS, S. 1977. Source mechanism of volcanic tremor — fluid-driven crack models and their application to 1963 Kilauea eruption. *Journal of Volcanology and Geothermal Research*, **2**, 259–287.

AKI, K. & RICHARDS, P. G. 2002. *Quantitative Seismology — 2nd edition*. University Science Books.

BARCLAY, J., RILEY, D. S. & SPARKS, R. S. J. 1995. Analytical models for bubble growth during decompression of high viscosity magmas. *Bulletin of Volcanology*, **57**, 422–431.

CAFLISCH, R. E., MIKSIS, M. J., PAPANICOLAOU, G. C. & TING, L. 1985*a*. Effective equations for wave-propagation in bubbly liquids. *Journal of Fluid Mechanics*, **153**, 259–273.

CAFLISCH, R. E., MIKSIS, M. J., PAPANICOLAOU, G. C. & TING, L. 1985*b*. Wave-propagation in bubbly liquids at finite volume fraction. *Journal of Fluid Mechanics*, **160**, 1–14.

CHOUET, B. 1986. Dynamics of a fluid-driven crack in 3 dimensions by the finite-difference method. *Journal of Geophysical Research (Solid Earth and Planets)*, **91**, 13967–13992.

CHOUET, B. 1988. Resonance of a fluid-driven crack — radiation properties and implications for the source of long-period events and harmonic tremor. *Journal of Geophysical Research (Solid Earth and Planets)*, **93**, 4375–4400.

CHOUET, B. A. 1996. Long-period volcano seismicity: its source and use in eruption forecasting. *Nature*, **380**, 309–316.

COLLIER, L., NEUBERG, J. W., LENSKY, N., LYAKHOVSKY, V. & NAVON, O. 2006. Attenuation in gas-charged magma. *Journal of Volcanology and Geothermal Research*, **153**, 21–36.

COMMANDER, K. W. & PROSPERETTI, A. 1989. Linear pressure waves in bubbly liquids — comparison between theory and experiments. *Journal of the Acoustical Society of America*, **85**, 732–746.

DINGWELL, D. B. 1998. Recent experimental progress in the physical description of silicic magma relevant to explosive volcanism. *In*: GILBERT, G. S. & SPARKS, R. S. G. (eds) *The Physics of Explosive Volcanic Eruptions*. Geological Society, London, Special Publication, **145**, 9–26.

HURWITZ, S. & NAVON, O. 1994. Bubble nucleation in rhyolitic melts — experiments at high-pressure, temperature, and water-content. *Earth and Planetary Science Letters*, **122**, 267–280.

ICHIHARA, M. & KAMEDA, M. 2004. Propagation of acoustic waves in a visco-elastic two-phase system: influences of the liquid viscosity and the internal diffusion. *Journal of Volcanology and Geothermal Research*, **137**, 73–91.

ICHIHARA, M., OHKUNITANI, H., IDA, Y. & KAMEDA, M. 2004. Dynamics of bubble oscillation and wave propagation in viscoelastic liquids. *Journal of Volcanology and Geothermal Research*, **129**, 37–60.

KELLER, J. B. & KOLODNER, I. I. 1956. Damping of underwater explosion bubble oscillations. *Journal of Applied Physics*, **27**, 1152–1161.

KELLER, J. B. & MIKSIS, M. 1980. Bubble oscillations of large-amplitude. *Journal of the Acoustical Society of America*, **68**, 628–633.

LENSKY, N. G., LYAKHOVSKY, V. & NAVON, O. 2001. Radial variations of melt viscosity around growing bubbles and gas overpressure in vesiculating magmas. *Earth and Planetary Science Letters*, **186**, 1–6.

LENSKY, N. G., LYAKHOVSKY, V. & NAVON, O. 2002. Expansion dynamics of volatile-supersaturated liquids and bulk viscosity of bubbly magmas. *Journal of Fluid Mechanics*, **460**, 39–56.

LENSKY, N. G., NAVON, O. & LYAKHOVSKY, V. 2004. Bubble growth during decompression of magma: experimental and theoretical investigation. *Journal of Volcanology and Geothermal Research*, **129**, 7–22.

LEZZI, A. & PROSPERETTI, A. 1987. Bubble dynamics in a compressible liquid. 2. 2nd-order theory. *Journal of Fluid Mechanics*, **185**, 289–321.

LYAKHOVSKY, V., HURWITZ, S. & NAVON, O. 1996. Bubble growth in rhyolitic melts: experimental and numerical investigation. *Bulletin of Volcanology*, **58**, 19–32.

MALVERN, L. E. 1969. *Introduction to the Mechanics of a Continuous Medium*. Prentice-Hall.

MOURTADA-BONNEFOI, C. C. & MADER, H. M. 2001. On the development of highly-viscous skins of liquid around bubbles during magmatic degassing. *Geophysical Research Letters*, **28**, 1647–1650.

MUNGALL, J. E., BAGDASSAROV, N. S., ROMANO, C. & DINGWELL, D. B. 1996. Numerical modelling of stress generation and microfracturing of vesicle walls in glassy rocks. *Journal of Volcanology and Geothermal Research*, **73**, 33–46.

NAVON, O. & LYAKHOVSKY, V. 1998. Vesiculation processes in silicic magmas. *In*: GILBERT, G. S. & SPARKS, R. S. G. (eds) *The Physics of Explosive Volcanic Eruptions*. Geological Society, London, Special Publication, **145**, 27–50.

NEUBERG, J., LUCKETT, R., BAPTIE, B. & OLSEN, K. 2000. Models of tremor and low-frequency earthquake swarms on Montserrat. *Journal of Volcanology and Geothermal Research*, **101**, 83–104.

O'CONNELL, R. & BUDIANSKY, B. 1978. Measures of dissipation in viscoelastic media. *Geophysical Research Letters*, **5**, 5–8.

PROSPERETTI, A., CRUM, L. A. & COMMANDER, K. W. 1988. Nonlinear bubble dynamics. *Journal of the Acoustical Society of America*, **83**, 502–514.

PROSPERETTI, A. & LEZZI, A. 1986. Bubble dynamics in a compressible liquid. 1. 1st-order theory. *Journal of Fluid Mechanics*, **168**, 457–478.

PROUSSEVITCH, A. A. & SAHAGIAN, D. L. 1996. Dynamics of coupled diffusive and decompressive bubble growth in magmatic systems. *Journal of Geophysical Research (Solid Earth)*, **101**, 17447–17455.

PROUSSEVITCH, A. A., SAHAGIAN, D. L. & ANDERSON, A. T. 1993. Dynamics of diffusive bubble-growth in magmas — isothermal case. *Journal of Geophysical Research (Solid Earth)*, **98**, 22283–22307.

ROMANO, C., MUNGALL, J. E., SHARP, T. & DINGWELL, D. B. 1996. Tensile strengths of hydrous vesicular glasses: An experimental study. *American Mineralogist*, **81**, 1148–1154.

VAN WIJNGAARDEN, L. 1968. On the equations of motion for mixtures of liquid and gas bubbles. *Journal of Fluid Mechanics*, **33**, 465–474.